A Machine Learning-Based Framework for Bias Correction of Doppler Weather Radar Observations

Vaibhav Tyagi, *Member, IEEE*, and Saurabh Das, *Senior Member, IEEE*

***Abstract*—Radar constant miscalibration is one of the major sources of uncertainty in the radar-derived rainfall products. The traditional bias correction techniques often struggle to account for the nonstationary and nonlinear nature of bias. This study proposes a novel machine learning-based framework using the extreme gradient boosting (XGBoost) algorithm to model reflectivity bias as a function of ground radar (GR) and spaceborne radar (SR) reflectivity differences, along with radar geometrical parameters (range, azimuth, and elevation). Furthermore, a strategy for near real-time bias correction is proposed based on an ensemble approach that combines an offline-pretrained model with an adaptive online learning component, incrementally updating the output as new data becomes available. This allows the model to adapt to evolving bias patterns over time. The results indicate that the proposed technique consistently outperforms the traditional iterative method. The results point toward its potential in reducing bias in near real-time for improved quantitative precipitation estimation (QPE) and other applications.**

***Index Terms*—Calibration, ensemble method, extreme gradient boosting (XGBoost), global precipitation measurement (GPM), machine learning, spaceborne radar (SR), weather radar.**

I. Introduction

POLARIMETRIC Doppler weather radars (DWRs) have significantly enhanced precipitation measurements by providing high-resolution observations with polarimetric variables that offer valuable insights into hydrometeor size, shape, concentration, and phase. It offers unprecedented opportunities across applications such as storm tracking, nowcasting, and quantitative precipitation estimation (QPE). Accurate QPE can aid improved numerical weather prediction (NWP) models as well in disaster management and early warning [1]. However, the quality of DWR observations significantly affects their quantitative use in various applications [2].

There are various sources of uncertainties that affect the DWR measurements, arising from rain microphysics as well as from a system point of view. Ground clutter, like tall buildings and mountains within the radar coverage, can significantly contaminate the received signal and become more pronounced in cases of complex topography. Attenuation of the transmitted signal is another factor contributing to the uncertainties in radar-derived rainfall products. Typically, DWRs operating at higher frequencies, such as X, C, and Ka bands, experience more pronounced attenuation effects. While polarimetric radar provides improvement in radar QPE, given the large number of single-polarized radars, the role of the calibration constant remains a major factor influencing the accuracy of radar-derived products. Houze et al. [3] reported that even a 2-dB calibration offset could lead to a 30% error in monthly rainfall estimates.

Typically, radar operators calibrate the radar using targets of known reflectance, like metallic spheres. However, these approaches are labor- and time-intensive, which limits their usage and often prevents them from being performed regularly. Advancements in spaceborne precipitation radars provide a cost-efficient opportunity to evaluate and calibrate DWR systems independently. These spaceborne systems are constantly monitored, having extensive internal and external calibration procedures with the errors in reflectivity ranging below 1 dBZ [4]. Several previous studies have focused on validating and calibrating ground radars (GR) using spaceborne radar (SR) observations, particularly with the dual-frequency precipitation radar (DPR) onboard the global precipitation measurement (GPM) mission [5].

The traditional bias correction procedures are based on least-squares techniques and iterative methods, which typically assume stationarity and linear bias characteristics. In practice, radar calibration biases could be nonlinear in nature and nonstationary over time due to hardware aging, maintenance activity, and operational changes. This makes conventional approaches inadequate for robust long-term calibration.

To overcome these challenges, a novel machine learning-based calibration framework is proposed using the extreme gradient boosting (XGBoost) algorithm that accounts for nonlinear and nonstationary biases in GR. Apart from GR–SR reflectivity differences, radar geometrical parameters (range, azimuth, and elevation) are also considered as input features, enabling the algorithm to capture spatial heterogeneity to account for GR–SR volume mismatch. Furthermore, a strategy is proposed based on an ensemble approach that combines an offline pretrained model and an online model to dynamically correct the bias for near real-time applications.

II. Datasets

A. Doppler Weather Radar

To evaluate the proposed methodology, the observations from the C-band (5.6–5.65 GHz) DWR located at

Received 2 December 2025; revised 13 February 2026; accepted 19 February 2026. Date of publication 23 February 2026; date of current version 5 March 2026. This work was supported in part by the Oceansat-03 Utilization Program by the Space Application Center (SAC), Indian Space Research Organisation (ISRO), Ministry of Earth Sciences (MoES) National Radar Meteorology Program under Grant MoES/16/04/2021-RDESS/NARM-4 and in part by the ISRO RESPOND Program under Grant RES-VSSC-2023-036. The work of Vaibhav Tyagi was supported by the University Grant Commission (UGC) for Providing Ph.D. Fellowship. *(Corresponding author: Saurabh Das.)*

The authors are with the Department of Astronomy, Astrophysics and Space Engineering, IIT Indore, Indore, Madhya Pradesh 453552, India (e-mail: das.saurabh01@gmail.com; saurabh.das@iiti.ac.in).

This article has supplementary downloadable material available at https://doi.org/10.1109/LGRS.2026.3667319, provided by the authors.

Digital Object Identifier 10.1109/LGRS.2026.3667319

the Thumba Equatorial Rocket Launching Station (TERLS; 8.53°N, 76.86°E) in Thiruvananthapuram, India, are used. The details of the radar system and its initial validation results can be found in [8].

The DWR dataset covers the period 2017–2024, and the data availability across this period is summarized in Table I (Supplementary Material). Specifically, radar data were unavailable for September and November 2020 and July 2021, while all other months contained sufficient data. All available Level-2 (L2A) plan position indicator (PPI) scans are used in the study obtained from the Meteorological and Oceanographic Satellite Data Archival Centre (MOSDAC, https://www.mosdac.gov.in).

B. GPM Dual-Frequency Precipitation Radar

The data from the GPM-DPR, operating at the Ka-band (35.5 GHz) and Ku-band (13.6 GHz), is used in the present study. It has a swath of 120 km with a horizontal resolution of 5 km and a vertical resolution of 125 m. The data is obtained from NASA's Earthdata portal (https://www.earthdata.nasa.gov/).

III. Methodology

A. Problem Formulation

The primary objective is to model and correct the bias between GR (Z_{GR}) and SR reflectivity (Z_{SR}). One of the major sources of the difference is the drifting of the radar constant, C, along with factors like the alignment geometry and spatiotemporal mismatch. The overall bias can be expressed as

$$B = C_{drift} + \epsilon \tag{1}$$

where C_{drift} denotes the drift of the radar constant and ϵ is the contribution from other random or unmodeled factors.

Warren et al. [6] demonstrated that the volume matching method (VMM) results combined with the radar maintenance logs can be useful to identify potential variations in GR calibration offsets. However, in the absence of any maintenance logs, it is practically challenging to model the effect of GR calibration offset arising solely from radar constant drift. Thus, the bias is modeled as integrated bias by constructing a mapping function that estimates the overall bias B as a function of relevant predictors and framed as a supervised regression problem

$$\min_{f\in\mathcal{F}} \mathbb{E}\left[(b - f(x))^2\right], \quad \text{s.t. } f \in \mathcal{F}_{\text{XGB}} \tag{2}$$

where $\mathcal{F}_{\text{XGB}}$ represents the hypothesis space, b is the difference of GR and SR ($Z_{GR} - Z_{SR}$), and $f(x)$ is the function to model the bias.

B. Preprocessing of GR and SR Data

The reading and preprocessing of raw GR data is performed using an in-house developed open-source Python library, Python Indian weather radar (PYIWR) toolkit [9] available at https://github.com/nitigsingh/pyiwr. The radar is located in the complex topography of the Western Ghats (high mountain ranges), resulting in significant contamination of reflectivity echoes due to ground clutter. To address this, a clutter correction algorithm proposed by Tyagi and Das [10] has been applied. It eliminates persistent ground clutter using a clutter map based on long-term observations along with a spatial filter based on horizontal variation of reflectivity, as shown in Fig. S1.

Furthermore, since both the instruments have different operating frequencies, the SR Ku-band reflectivity values are converted to GR C-band reflectivity using the procedure as outlined by Sharma and Kannan [11] based on empirical relations [12].

C. GR–SR Volume Matching

To quantitatively compare the GR and SR observations, the difference in the geometry and sampling technique of the two instruments needs to be considered. The VMM, as proposed by Schwaller and Morris [7], is used to collocate GR and SR observations. To enable reliable comparisons, a temporal tolerance of 5 min is considered. The collocated dataset is further filtered by considering quality rainy observations with successful bright band detection and by excluding the observations within the melting layer to avoid contamination from mixed-phase conditions [6].

D. Proposed Bias Correction Technique

To correct the GR bias using SR as a reference, a supervised bias correction framework is proposed to model the bias as a function of GR–SR reflectivity differences and radar geometrical parameters (range, azimuth, and elevation). The inclusion of these parameters enables the model to account for bias arising due to GR–SR volume mismatch, sampling effects, and spatial variability. The feature set is limited to radar-derived quantities to maintain a self-constrained framework that relies solely on DWR-based information. To model the bias, the XGBoost algorithm [13] is employed, due to its robustness to multicollinearity, ability to capture nonlinear dependencies, and computational efficiency. XGBoost has been widely shown to outperform other ensemble and deep learning methods for tabular data [15], making it well-suited for the present bias correction problem. Moreover, a comparative analysis for the year 2024 also reveals the superior performance of XGBoost, achieving the lowest root-mean-squared error (RMSE) (2.47 dBZ), mean absolute error (MAE) (1.64 dBZ), and highest correlation coefficient (CC) (0.89), outperforming random forest (RMSE: 2.64 dBZ, MAE: 1.75 dBZ, and CC: 0.87) and ridge regression (RMSE: 4.64 dBZ, MAE: 3.15 dBZ, and CC: 0.60). Before training the XGBoost model, hyperparameters such as the number of estimators, maximum tree depth, and learning rate are optimized using the RandomizedSearchCV function in scikit-learn. The model is trained and evaluated using a tenfold cross-validation strategy, ensuring a robust and unbiased estimate of model performance. The detailed flow of the process is illustrated in Fig. 1.

E. Real-Time Bias Correction Strategy

The proposed framework employs an ensemble bias correction approach that combines a pretrained model with an online model for real-time bias correction. The optimization is carried out globally, and a temporal validation strategy

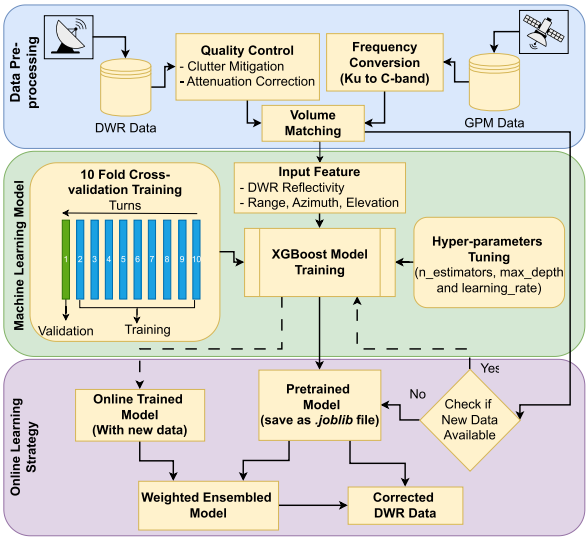

Fig. 1. Flowchart illustrating the proposed online learning bias correction framework. The diagram outlines the preprocessing, model training, and correction steps.

is adopted, wherein the model is trained on earlier years and tested on subsequent years to emulate real-time bias correction. The pretrained model, trained on historical data, serves as the baseline correction. In parallel, an online model is continuously updated and trained using a fixed N samples, in which new samples (n) are sequentially injected as and when available.

The ensemble model output is calculated as a weighted sum of the pretrained and online model outputs. The weights are adaptively optimized during the online learning phase by minimizing the mean squared error of the ensemble output. This adaptive weighting ensures that the ensemble places greater reliance on the pretrained model when recent data is limited or sparse, and gradually shifts toward the online model as new data becomes available.

IV. Results

A. Interannual Variability in Bias

The GR–SR volume matching is performed on the data from 2017 to 2024, resulting in a total of 25 645 samples. Based on this dataset, the interannual variability in the bias is analyzed first. Fig. 2 shows the annual variation of mean bias (MB) with the black curve and the number of samples in each year as blue bars. It is clear that MB, before correction, reveals significant interannual variability between 2017 and 2024. In 2017, the MB was relatively low (∼−3 dBZ) and gradually increased in magnitude, reaching a maximum value of nearly −11 dBZ in 2020. The year 2022 exhibits a different trend with an MB of around (∼−5.3 dBZ). To investigate this, the number of samples across each year is examined, as shown in Fig. 2. The year 2022 had a very limited sample (437), which could be the possible reason for this different trend.

The observed interannual variability suggests that the GR–SR bias is not temporally stationary. The potential contributors to this variability include gradual radar miscalibration,

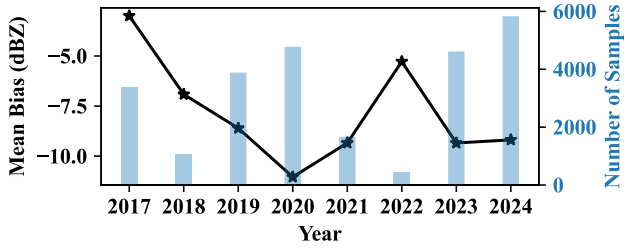

Fig. 2. (Left) Yearly variation of MB before correction (black stars, *y*-axis) and the (right) corresponding number of samples (blue bars, *y*-axis).

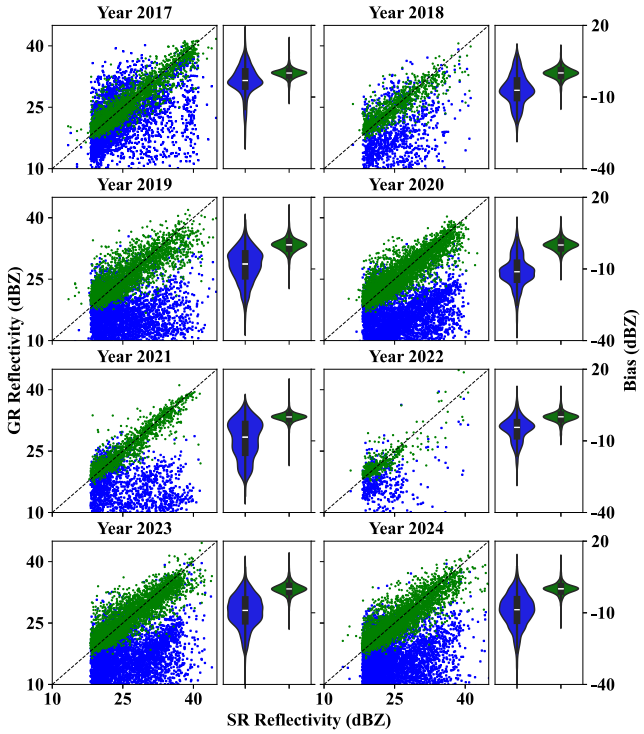

Fig. 3. Scatterplots of radar reflectivity and violin distributions of bias for each year. (Left) Each subplot shows scatterplots of spaceborne radar (SR) reflectivity against GR reflectivity before (blue) and after (green) bias correction, with the 1:1 reference line indicated. (Right) Each subplot shows violin plots of the corresponding bias distributions.

lack of calibration activities, and hardware aging. This emphasizes the need for periodic bias assessment to maintain consistency across the time series.

B. Bias Correction

The collocated data is segregated based on year, and the model training is performed for individual years. Fig. 3 shows the scatter plot of GR and SR reflectivity before (blue) and after (green) correction, along with the probability distributions of the bias. The scatter plots and bias distributions clearly demonstrate the effectiveness of the proposed bias correction method across different years. Before correction, GR reflectivity is generally negatively biased relative to SR, as evidenced by the systematic offset from the 1:1 reference line. After the correction, the GR reflectivity values significantly improved with green scatter points lying mostly around the 1:1 line. The violin plots further illustrate that the bias distributions are

TABLE I

YEARLY STATISTICS: CC, MB, MAE, AND RMSE BEFORE AND AFTER CORRECTION (ITERATIVE AND XGBOOST METHODS)

Year	Samples	Before Correction				Iterative Method				Proposed Method			
		CC	MB	MAE	RMSE	CC	MB	MAE	RMSE	CC	MB	MAE	RMSE
2017	3367	0.449	-2.998	5.138	6.822	0.449	-1.288	4.596	6.262	0.927±0.007	-0.006±0.144	1.460±0.035	2.121±0.087
2018	1063	0.379	-6.914	7.894	9.388	0.379	-0.154	4.930	6.352	0.842±0.036	-0.028±0.252	1.805±0.185	2.557±0.272
2019	3885	0.077	-8.603	9.046	11.113	0.077	0.487	5.716	7.051	0.841±0.023	-0.002±0.193	2.079±0.123	2.919±0.200
2020	4777	0.271	-11.036	11.286	12.822	0.271	1.514	5.062	6.700	0.879±0.013	0.002±0.091	1.875±0.099	2.577±0.137
2021	1668	-0.065	-9.340	9.734	12.155	-0.065	-4.170	6.940	8.826	0.931±0.020	-0.065±0.231	1.337±0.129	2.054±0.304
2022	437	0.318	-5.280	5.809	7.333	0.318	0.150	3.878	5.090	0.837±0.063	0.000±0.338	1.611±0.204	2.359±0.481
2023	4616	0.273	-9.342	9.650	11.502	0.273	2.618	5.854	7.203	0.888±0.011	-0.011±0.165	1.848±0.090	2.596±0.129
2024	5832	0.142	-9.184	9.586	11.604	0.142	-2.214	5.706	7.431	0.887±0.008	-0.000±0.127	1.638±0.045	2.368±0.091

MB, MAE , and RMSE are expressed in DBZ.

broad and skewed before correction and become significantly narrower afterward, with their MB close to zero. This indicates that the proposed correction schemes reduce the MB and also improve the consistency between GR and SR.

Table I presents the yearly performance metrics (CC, MB, MAE, and RMSE) before and after correction, along with results from a widely used iterative correction method for comparison [6]. Uncertainties for all metrics are reported as 95% confidence intervals computed across ten cross-validation folds of the training data. A p-value for all metrics was found to be less than 0.05 using a paired t-test, confirming that the improvements are statistically significant. Before correction, the GR–SR comparison shows weak correlations (often <0.5 and even negative for the year 2021), large negative MB (ranging from −3 dBZ in 2017 to around −11 dBZ in 2020), and high MAE and RMSE values. This indicates a substantial underestimation of GR reflectivity relative to SR measurements and poor consistency between the two. After correction, the CCs increase substantially (>0.82, reaching up to 0.93 in 2021), MB is effectively removed (values close to zero), and MAE values are below 2.1 dBZ. A significant drop in RMSE values is also observed.

As shown in Table I, while the iterative method does reduce absolute MB, the CCs remain unchanged and are very low. The MAE and RMSE are also considerably high. This indicates that the iterative method is less effective in capturing bias between SR and GR reflectivity. In contrast, the proposed technique consistently achieves superior performance across all years. The proposed technique significantly reduces the spatial bias variability (Fig. S2). Although yearly results appear consistently high, they may reflect overfitting to year-specific patterns, thereby motivating the development of an online–offline strategy to improve robustness and cross-year generalization.

C. Sensitivity Analysis

While the proposed technique shows promising results, its sensitivity to input data must be considered for broader applicability and generalizability. A sensitivity analysis is performed using data from 2024, which comprises a total of 5832 samples. The model is trained by varying the size of the input data, and the corresponding MB and MAE are evaluated (Fig. 4). The sensitivity analysis reveals that the performance of the technique is sensitive to the number of input samples. At very low sample sizes, both the MB and MAE exhibit fluctuations, reflecting unstable correction behavior. As the sample size increases, the MB converges toward zero, and the MAE decreases significantly. After approximately 1000 samples, the MB converges slowly to zero, and the MAE is also below 2 dBZ.

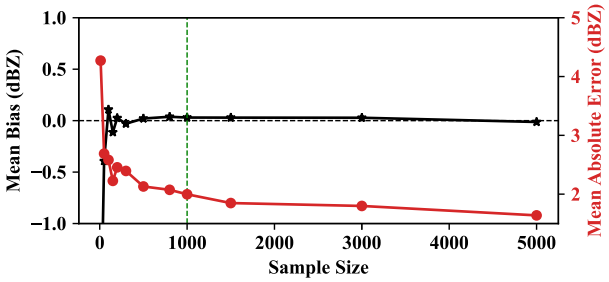

Fig. 4. Variation of MB (black curve) and MAE (red curve) with different input data size.

D. Implementation Strategy for Real-Time Bias Correction

The sensitivity study indicates the potential for implementing the proposed technique for real-time correction. For this, an online-learning framework is used and tested for the year 2023. The online learning began by initializing the model with 2000 matched samples (N), and a rolling window is considered to inject the new incoming data (n = 500 samples) as and when available. After each iteration, the model is evaluated on the next 1000-sample test chunk. This approach allows a new model to be retrained periodically, incorporating new observations to refine its performance. The ensemble of online learning model output and the pretrained model (trained using data from 2017 to 2022, around 15 197 samples in this case) is calculated using the weighted average of these two models.

The performance of the ensemble model and the pretrained-only model is compared in Fig. 5. The figure presents the MB (plain bars), MAE (dotted bars), and RMSE (hashed bars) for the raw (blue), pretrained (orange), and ensemble (green) models across successive iterations. The results demonstrate that the ensemble model, considering both pretrained offline and online models, progressively adapts to changes in data over time, with a significant reduction in all metrics after the injection of the new data, as shown by the green bars. This suggests the suitability of the framework for real-time bias correction with the availability of new incoming data.

V. DISCUSSION AND CONCLUSION

Several studies worldwide have focused on calibrating and evaluating the performance of GR networks [5], [6], [7]. The present study proposes a machine learning-based framework for correcting biases in GR data in near real-time using

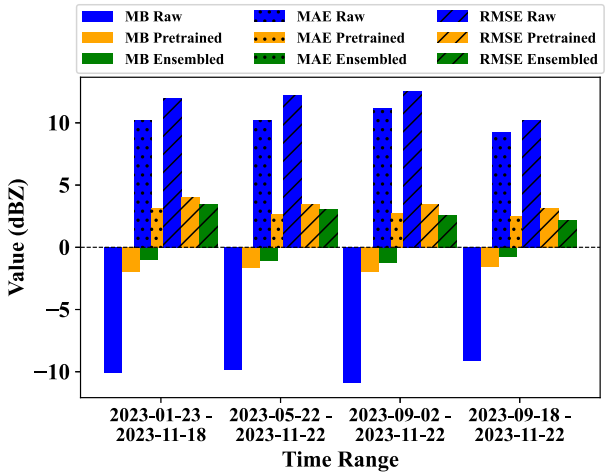

Fig. 5. Comparison of the MB in dBZ with the pretrained model (orange bars) and ensembled model (green bars) over successive iterations. The raw MB before any correction is shown with blue bars. The x-axis represents the start and end times of the test data period.

well-calibrated SR reflectivity data as a reference. The initial assessment of bias in the TERLS C-band GR before correction reveals significant variability in the MB. The bias is minimal in 2017 but increases in magnitude in the subsequent years, exhibiting notable interannual variability. While infrequent calibration activities may contribute to the drift in calibration offset, years with limited sample availability could also affect the robustness of the estimated bias.

The proposed technique demonstrated substantial improvements in error metrics by reducing the MB, RMSE, and MAE, while improving CCs between GR and SR reflectivity. After applying the proposed technique, the CC improved significantly from an average of 0.23 to 0.88 (across all years). The bias before correction exhibits a broad distribution, suggesting the nonlinear characteristics of the same. The application of a uniform bias is thus ineffective, as also observed in Table I, by the poor performance of the iterative method. While the iterative approach applies a uniform adjustment based on the estimated bias, the proposed machine learning framework can learn the underlying bias patterns and apply the nonlinear corrections. Thus, the proposed technique outperforms the iterative correction method. Similar observations are also reported by several other researchers for diverse bias correction applications [14]. The proposed approach achieves a postcorrection CC of 0.88, compared with the value of 0.79 as reported by [11] for their CNN-based bias-correction framework for Delhi DWR.

The study also proposes a real-time bias correction strategy using a historical pretrained model (offline model) and online learning based on new incoming SR observations (online model) to continuously improve the model performance, significantly reducing the MB as new observations are incrementally injected. This highlights the framework's robustness and suitability for real-time bias correction in operational settings.

In the present study, the framework is demonstrated using a single C-band radar; however, it can be applied to other ground-based radars through site-specific retraining to account for differences in radar characteristics and climatological regimes. The effectiveness of the approach depends on the availability and quality of SR reference data, appropriate tuning for geographic location, and operational factors such as real-time data latency. Future work could explore the incorporation of polarimetric radar parameters and physics-based modeling approaches.

REFERENCES

[1] V. Chandrasekar, H. Chen, and B. Philips, "Principles of high-resolution radar network for hazard mitigation and disaster management in an urban environment," *J. Meteorological Soc. Japan. Ser. II*, vol. 96, no. 1, pp. 1–20, 2018. [Online]. Available: https://doi.org/10.2151/jmsj.2018-015

[2] D. Michelson, B. Hansen, D. Jacques, F. Lemay, and P. Rodriguez, "Monitoring the impacts of weather radar data quality control for quantitative application at the continental scale," *Meteorological Appl.*, vol. 27, no. 4, p. 1929, Jul. 2020. [Online]. Available: https://doi.org/10.1002/met.1929

[3] R. A. Houze Jr., S. Brodzik, C. Schumacher, S. E. Yuter, and C. R. Williams, "Uncertainties in oceanic radar rain maps at kwajalein and implications for satellite validation," *J. Appl. Meteorol.*, vol. 43, no. 8, pp. 1114–1132, Aug. 2004. [Online]. Available: https://doi.org/10.1175/1520-0450(2004)043<1114:UIORRM>2.0.CO;2

[4] N. Takahashi, H. Kuroiwa, and T. Kawanishi, "Four-year result of external calibration for precipitation radar (PR) of the tropical rainfall measuring mission (TRMM) satellite," *IEEE Trans. Geosci. Remote Sens.*, vol. 41, no. 10, pp. 2398–2403, Oct. 2003. [Online]. Available: https://doi.org/10.1109/TGRS.2003.817180

[5] S. K. Biswas and V. Chandrasekar, "Cross-validation of observations between the GPM dual-frequency precipitation radar and ground based dual-polarization radars," *Remote Sens.*, vol. 10, no. 11, p. 1773, Nov. 2018. [Online]. Available: https://doi.org/10.3390/rs10111773

[6] R. A. Warren et al., "Calibrating ground-based radars against TRMM and GPM," *J. Atmos. Ocean. Technol.*, vol. 35, no. 2, pp. 323–346, Feb. 2018. [Online]. Available: https://doi.org/10.1175/JTECH-D-17-0128.1

[7] M. R. Schwaller and K. R. Morris, "A ground validation network for the global precipitation measurement mission," *J. Atmos. Ocean. Technol.*, vol. 28, no. 3, pp. 301–319, Mar. 2011. [Online]. Available: https://doi.org/10.1175/2010JTECHA1403.1

[8] K. K. Kumar et al., "C-band dual-polarization Doppler weather radar at Thumba (8.537°N, 76.865°E): Initial results and validation," *J. Appl. Remote Sens.*, vol. 14, no. 4, Nov. 2020, Art. no. 044509. [Online]. Available: https://doi.org/10.1117/1.JRS.14.044509

[9] N. Singh, V. Tyagi, S. Das, U. K. Sahoo, and S. S. Kundu, "Python Indian weather radar toolkit (pyiwr): An open-source Python library for processing, analyzing and visualizing weather radar data," *J. Comput. Sci.*, vol. 81, Sep. 2024, Art. no. 102363, doi: 10.1016/j.jocs.2024.102363.

[10] V. Tyagi and S. Das, "A probabilistic algorithm for mitigating persistent ground clutter in Doppler weather radar," *J. Geophys. Res., Atmos.*, vol. 130, no. 15, p. 2025, Aug. 2025, doi: 10.1029/2025jd043478.

[11] A. Sharma and S. R. Kannan, "Intercomparison between IMD ground radar and TRMM PR observations using alignment methodology and artificial neural network," *J. Earth Syst. Sci.*, vol. 130, no. 1, pp. 20, Dec. 2021. [Online]. Available: https://doi.org/10.1007/s12040-020-01540-8

[12] Q. Cao et al., "Empirical conversion of the vertical profile of reflectivity from Ku-band to S-band frequency," *J. Geophys. Res., Atmos.*, vol. 118, no. 4, pp. 1814–1825, Feb. 2013. [Online]. Available: https://doi.org/10.1002/jgrd.50138

[13] T. Chen and C. Guestrin, "XGBoost: A scalable tree boosting system," in *Proc. 22nd ACM SIGKDD Int. Conf. Knowl. Discovery Data Mining*, Aug. 2016, pp. 785–794. [Online]. Available: https://doi.org/10.1145/2939672.2939785

[14] H. Chen, L. Sun, R. Cifelli, and P. Xie, "Deep learning for bias correction of satellite retrievals of orographic precipitation," *IEEE Trans. Geosci. Remote Sens.*, vol. 60, pp. 1–11, 2022. [Online]. Available: https://doi.org/10.1109/TGRS.2021.3105438

[15] R. Shwartz-Ziv and A. Armon, "Tabular data: Deep learning is not all you need," *Inf. Fusion*, vol. 81, pp. 84–90, May 2022. [Online]. Available: https://doi.org/10.1016/j.inffus.2021.11.011